Journal of The
Electrochemical Society

Surface Modification Improves Spinel $LiCoO_2$ Li-Ion Battery Cathode Materials Grown by Low Temperature Solvothermal Flow Reaction

To cite this article: Yan Zhang *et al* 2024 *J. Electrochem. Soc.* **171** 010531

Journal of The Electrochemical Society, 2024 **171** 010531

Surface Modification Improves Spinel $LiCoO_2$ Li-Ion Battery Cathode Materials Grown by Low Temperature Solvothermal Flow Reaction

Yan Zhang,[1] Umair Gulzar,[1] Alex Lonergan,[1] Alex Grant,[1] Aoife Carroll,[1] Ahin Roy,[2,3] Valeria Nicolosi,[2,3] Tony D. Keene,[4] and Colm O'Dwyer[1,2,3,5,*,z]

[1]*School of Chemistry, and Tyndall National Institute, University College Cork, Cork, T12 YN60, Ireland*
[2]*School of Chemistry, Trinity College Dublin, Dublin 2, Ireland*
[3]*AMBER Research Center, Trinity College Dublin, Dublin 2, Ireland*
[4]*School of Chemistry, University College Dublin, Belfield, Dublin 4, Ireland*
[5]*Environmental Research Institute, University College Cork, Cork T23 XE10, Ireland*

Methods that provide routes to $LiCoO_2$ growth with lower energy requirements from recycled battery cathode ashes are important for sustainable Li-ion battery technology . Here, a low temperature route to a stable, coated spinel-phase LT-LCO material with secondary Co_3O_4 phase can be achieved at 300 °C directly from the layered double hydroxide $[Li_2(ox)_2][Co_5(OH)_8]$ product of solvothermally synthesized LiOH and $CoCl_2$. The low-temperature $LiCoO_2$ materials (known as LT-LCO) consist of spinel-phase LCO and secondary Co_3O_4 phase. As a cathode in lithium batteries, we used a solution-based method of coating with an ionic conductor $LiAlO_2$ with AlF_3 to mitigate sluggish reversible lithiation kinetics and the poor cycling and rate performance of as-synthesized spinel LT-LCO. The coating modification promotes reversible lithium ion transfer and stabilizes the spinel structure. The modified LT-LCO cathode has significantly better overall capacity and rate performance, with a capacity retention of ~80 mAh g^{-1} after 150 cycles (factoring the LT-LCO and Co_3O_4 mass). The initial first cycle coulombic efficiency significantly improves to >95%. The data show that even spinel phase LCO grown by this solvothermal route cycles stably with a useful specific capacity and rate response in the voltage range 2.0–4.2 V.

 [DOI: 10.1149/1945-7111/ad1e41]

Manuscript submitted October 25, 2023; revised manuscript received December 15, 2023. Published January 29, 2024.

Supplementary material for this article is available online

Rechargeable lithium-ion batteries (LIBs) technology has revolutionized various portable industrial electronics ranging from cell phone to electro-mobility because of high specific energy/power output and good cycle ability.[1–4] Lithium cobalt oxide ($LiCoO_2$, LCO) as the first commercialized remains an important cathode material because of its well-balanced performance when paired with graphitic anodes in organic electrolytes.[5–7] The dominant commercialized LCO cathode has a hexagonal crystalline phase with a layered-rhombohedral α-$NaFeO_2$ structure with an R3m space group.[8,9] This configuration consists of alternate cobalt and lithium layered crystal structure that favors efficient intercalation/de-intercalation of lithium ions, giving a high theoretical specific capacity of 274 mAh g^{-1}. However, the synthesis of layered LCO cathode is typically carried out by firing at high temperature >800 °C over a period of several days (HT-LCO). The conditions of high temperature treatment with long reaction times can sometimes limit the control of the reaction process, requiring appropriate high temperature infrastructure and associated energy costs overall, including the sintering step. And in practical applications, its specific capacity of HT-LCO cathode is inherently limited to about 50% of the theoretical value because of the reversible extraction of ~0.5 Li ions per mole of the oxide and the destabilization of the structure when it is fully oxidized.[5,10,11] HT-LCO, the $LiCoO_2$ used in many cells currently, intrinsically suffers from relatively poor cycle life due to irreversible phase transitions, cathode electrolyte interphase and complex interfacial instability,[11] but the advent of electrolyte additives[12,13] and other strategies can mitigate some limitations and this material now performs quite well.

By comparison, the synthesis and electrochemical response of LT-LCO in lithium batteries have received less attention since the material was first reported from a 400 °C process by Gummow et al. in 1992.[14] It was proposed that LT-LCO presented a rock-salt structure where only about 6% the cobalt ions in the lithium-rich layers and about 4% the lithium ions in the cobalt-rich layers and is somewhat unfavorable to fast lithium ion conductivity. Further investigations showed that the cation sites occupy the same position in HT-LCO and in the LT-LCO structure. In HT-LCO, however, the Li are group into layered alternating with those of Co, perpendicular to a single [111] direction. The Fd3m spinel structure has cations arranged in alternating layers perpendicular to all four of the ⟨111⟩ directions. LT-LCO was subsequently found to render in amorphous, spinel, or cubic phases, and some polymorphs, which have less perfectly ordered structure because of a lower activation energy from low temperature crystallization.[15–18] In general, the cubic phase with Fm3m symmetry is metastable; it prefers to form a new spinel compound $LiCo_2O_4$ by removal of a Li^+ from its octahedral site (cubic D4 structure) to a tetrahedral site, and this phase has very poor electrochemical activity.[18] The spinel phase with Fd3m symmetry is an ordered rock-salt structure with a cubic unit cell.[16] It generally exhibits a two-phase lithium storage mechanism between 3.2 and 3.9 V with ~0.45 Li^+ extraction and ~0.24 Li^+ reinsertion into the spinel phase, whereas the hexagonal LCO with its layered structure generally provides 0.5 Li^+ extraction/insertion in the voltage range 3.8–4.2 V.[17] It took a detailed examination of the LT-LCO phase together with electrochemical data to determine a spinel phase with a c/a ratio of the unit cell of 4.9, a so-called cation-disordered rock salt structure. During cycling, however, very few structural changes were observed in LT-LCO compared to HT-LCO, and the characteristic lower voltage plateau was attributed to a coexistence of two spinel phases: the spinel LT-LCO (almost isostructural with $Li_2Ti_2O_4$) and a spinel $Li_{0.5}CoO_2$.

The LT-LCO polymorph is reported to have the highest initial capacity, but it drops dramatically upon cycling to the point where it is a poor candidate for stable, multicycle applications.[19] Since the phase receives comparatively less attention compared to the layered LCO structure, there are still open questions on the mechanism for this capacity fading, whether catalytic decomposition of electrolyte occurs (LT-LCO has been shown recently to be an effective OER

*Electrochemical Society Member.
[z]E-mail: c.odwyer@ucc.ie

and ORR catalyst),[20] material degradation happens, or if cation mixing in the material occurs. At least in the synthetic protocol we report here, the HT-LCO component often found in LT-LCO synthesis is avoided, and as will be shown, surface modification improves the response. Overall, the LT-LCO material has been reported by many different synthetic methods, and due to its ability to form polymorphs, and a range of sizes/morphologies, the reported structures and their influence on electrochemical behavior in lithium cells varies. Many studies describe various electrochemical activities at a lower voltages for LT-LCO material compared to the layered HT-LCO material.[16,17,21] LT-LCO cathodes are often reported as having rapid capacity decay, low initial coulombic efficiency, poor rate performance and high self-discharge rate.[22] It does, however, operate a slightly lower voltages in its unmodified form, which is supposed to limit the degree of electrolyte decomposition during cycling. The sluggish kinetics of Li ion transfer at the surface and the structural instability of LT-LCO material during cycling are considered root cause of these issues. Its structure is less efficient at promoting Li intercalation compared to the layered HT-LCO,[23] and so some modification at the surface is needed to overcome this initial barrier and to improve the kinetics of cation access to the spinel structure and the associated charge compensation. In spite of that, sintering treatment at high temperature/pressure of LT-LCO material to form the layered rhombohedral HT-LCO material can be done, but has a considerable energy cost and time penalty.[19,24–26] Additionally, sintering approaches of LT-LCO can cause coarsening of the particles, which affects overall response and rate performance in Li-ion cells by the formation of much larger crystallites. A similar effect happens during the typical crystallization in O_2 at >900 °C during industrial HT-LCO manufacturing,[27] and alternative approaches are needed to improve LT-LCO since direct growth of HT-LCO from sol-gel,[28,29] precipitation,[30] hydrothermal methods and others[31] were ineffective. And there are very few reports that deal with modification to LT-LCO material to behave as a more stable battery cathode.

Modifications that include bulk doping (e.g., Mg, Cr, Ti, Mn, P and Al; Al/La co-doping), as well as surface coating layers (e.g., metal-oxide, -phosphates, -fluorides) have been shown to improve the cycle life and high-rate performance of commercial LCO materials.[32–40] Some of these surface doping and coating modifications limit direct contact between the LCO electrode surface and the electrolyte, retaining oxygen in the lattice and preventing, or at least reducing, transition metal dissolution[41] and parasitic reactions from oxygen redox. The result is usually the formation of a more stable cathode-electrolyte interphase structure, and a mitigation of material decomposition and catalytic decomposition of electrolyte species.[42] Very recent results show how coatings with these properties are excellent for high voltage cathodes, where cathode decomposition and surface-electrolyte interactions are a major issue in long term performance for these compounds.[43] For example, Yoon reported that bulk LCO particles with Ni doping exhibited superior stability and areal capacity in both coin-type half-cell and pouch-type full-cell.[34] Long-term cycling stability of 1000 cycles and higher rate capability are achieved in commercial LCO with MgF_2 doping. In the case of fluoride dopants, reports often cite improved surface structural integrity and that their inclusion into the LCO particles provides lithium ion intercalation/extraction channels. In the case of MgF_2, this is enabled by Mg pillars in the LCO structure. However, the most commonly reported effect of a dopant species that modifies the LCO structure is typically with HT-LCO phases and other cathode materials;[44–48] adapting a similar approach for the spinel structure while protecting the surface could be useful for the LT-LCO phase.[49] Other reports revealed that Li-ion conductive surface modification layers such as Li_2ZrO_3, Li_3PO_4 and $LiAlF_4$ not only alleviate the side reactions and transition metal dissolution to improve structural stability, but also provide a stable Li-ion conductive channel for faster ion migration to increase the Li-ion diffusion coefficient within the material.[37–40] Thus, a modification strategy and inclusion of a metal fluoride M–F (M = metal such as Mg, Al etc) is proposed in our work to improve overall electrochemical response of spinel phase LT-LCO cathodes during cycling at various rates. The surface modification approach tackles aforementioned issues and together a thin amorphous $LiAlO_2$ with AlF_3 coating should stabilize decomposition of the spinel LCO while improving its rate response with better ambipolar conductivity. Importantly, it could in principle limit oxygen redox and side reactions with the electrolyte, especially in the delithiated state, so that this new low temperature and battery ash recycling approach can provide useful performance in LT-LCO battery cathodes.

Here, we show how LT-LCO material can be crystallized at just 300 °C (onset of the process begins at 260 °C) from a layered double hydroxide $[Li_2(ox)_2][Co_5(OH)_8]$ that is solvothermally synthesized from a mixture of LiOH and $CoCl_2$ in oxalic acid for just 4 h. This reduces synthesis time and temperature for LT-LCO that is normally grown at 400 °C for 2–3 d, whereas HT-LCO requires at least 800 °C for 3–9 d, depending on the process and temperature. The approach was designed as part of work to provide a high volume and rapid protocol using LiOH as the starting material either in battery grade, or from ashes from Li-ion LCO cathode recycling that can be conducted continually in a flow reaction. The LT-LCO material is a spinel LCO phase mixed with a secondary Co_3O_4 phase in a 2:1 ratio. By developing a coating of $LiAlO_2$ and introduction of AlF_3, we show how a normally unstable and poorly cycling LT-LCO material can be significantly improved to become a stable electrode, with good rate response and a remarkable first cycle coulombic efficiency >95% in a voltage range of 2.0–4.2 V in coin cell lithium batteries.

Experimental

Low temperature solvothermal synthesis of LT-LCO.—The low temperature synthesis of $LiCoO_2$ is achieved by a solvothermal reaction of LiOH and $CoCl_2$ with oxalic acid in water at 200 °C. The product is a layered double hydroxide $[Li_2(ox)_2][Co_5(OH)_8]$. Calcination at 300 °C for 4 h gives $LiCoO_2$ and Co_3O_4 as inorganic products in a 2:1 ratio.[50] The process can be run as a continuous flow to produce the material.

The preparation of modified LT-LCO.—34.15 mg aluminium nitrate nonahydrate ($Al(NO_3)_3{\cdot}9H_2O$) and 6.3 mg lithium nitrate ($LiNO_3$) were dissolved in 15 ml deionized water and stirred for 2 h to form solution A. Separately, 14.15 mg ammonium fluoride (NH_4F) was dissolved completely in 10 ml deionized water and stirred for 2 h to form solution B. Then 500 mg of LT-LCO powder was added to solution A, and after stirring for 2 h, solution B was added to obtain a miscible mixture of LT-LCO precursor solution. The mixture was stirred constantly at 100 °C until evaporation of the solvent. The sample was dried in a convection oven at 80 °C overnight. The precursor-coated powder was collected and sintered at 300 °C for 5 h under vacuum ($\sim 10^{-2}$ mbar) with a heating rate of 5 °C min^{-1} from room temperature to yield the final sample.

Materials characterization.—The X-ray diffraction (XRD) patterns were recorded via a Philips Xpert PW3719 diffractometer with Cu Kα radiation (λ = 1.542 Å), which were used to confirm the crystalline structures of the composites. Raman scattering was performed with a Renishaw InVia Raman Spectrometer using a 30 mW Ar^+ laser at 514 nm excitation. The beam was focused onto the samples using a 50× objective lens and spectra were collected using a RenCam CCD camera. Scanning electron microscopy (SEM) analysis was performed using an FEI Quanta 650 FEG high resolution SEM at an accelerating voltage of 10 kV. The transmission electron microscopy (TEM), high-resolution TEM (HRTEM), selected area electron diffraction (SAED), nanobeam diffraction (NBD) patterns and high-angle annular dark-field (HAADF) images were acquired on a JEOL JEM-2100F electron microscope. High angle annular dark field TEM measurements and electron energy loss spectroscopic (EELS) mapping of electrode materials were

acquired using a FEI Titan 80 FEG S/TEM (80–300 kV). Electron Energy Loss Spectroscopy (EELS) was acquired using a Tridium 863 spectrometer with the energy dispersion set to 0.1 eV/channel. X-ray photoelectron spectroscopy was carried out using a Kratos AXIS ULTRA XPS. Core level scans were acquired with a step size of 0.05 eV, dwell time of 100 ms, with between 8–18 scans averaged at a pass energy of 20 eV from a monochromated Al Kα X-ray source at 300 W (20 mA, 15 kV) power. Data was processed using CasaXPS software where a Shirley background correction was employed.

Electrochemical measurements.—The electrodes were prepared using a traditional slurry coating procedure. The electrode was prepared via the mixture of as-prepared active material (LT-LCO or modified LT-LCO), conductive carbon (super-P) and polyvinylidene fluoride (PVDF) in the mass ratio of 8:1:1, dissolved in N-methyl-2-pyrrolidinone (NMP) to form a slurry. This slurry was uniformly painted on an aluminium foil and then dried in the vacuum oven at 120 °C for 12 h. After drying, it was punched into wafers with a diameter of 15 mm and used as the cathode for LIBs. In order to avoid the deterioration of the LCO electrodes, the LCO electrodes were placed in a water and oxygen-free Ar-atmosphere glove box. The lithium storage performance was estimated by El-Cell, where the lithium metal acts as the counter electrode, glass fiber (El-Cell ECC1–01–0012-A/L) is used as the separator. The electrolyte consisted of 1.0 M of $LiPF_6$ dissolved in EC/DMC solution (1/1, v/v). The half cells were assembled in an Ar-filled glove box (Inert I-Lab) where water/oxygen content is lower than 1 ppm. The cyclic voltammetry (CV) data and the galvanostatic charge-discharge cycling performance tests were carried out on a BioLogic VSP Potentiostat/Galvanostat.

Results and Discussion

Morphology and structure.—The solvothermal flow synthesis process for preparation of LT-LCO is shown in Fig. 1. Analytical grade LiOH and Co_3O_4 are mixed with oxalic acid in water at 200 °C. The resulting layered double hydroxide $[Li_2(ox)_2][Co_5(OH)_8]$ was calcined at 300 °C for 4 h to form the LT-LCO and Co_3O_4 product. The initial precursors here are pure LiOH and $CoCl_2$, but the process can use recycled ashes from LCO battery cathodes. Surface modification is performed on the LT-LCO material as described in the Experimental section. Given the limitations of LT-LCO in terms of voltage fade, capacity fade and slower kinetics that affect stable rate response, we developed facile coating method to grown $LiAlO_2$ and AlF_3 to improve electrochemical response and stabilize the electrode and the interface with the electrolyte. This coating approach is chosen to (a) keep the LT-LCO phase inactive during charging, (b) prevent or at least limit O migration to the electrolyte, (c) avoid (electro)catalytic behavior, and (d) be a reasonably good electronic and ionic conductor during charging and discharging to offset the slower kinetics of the intercalations reactions with the spinel LCO phase.

The X-ray-diffraction (XRD) measurements were performed to confirm the crystalline structure of the synthesized powders. As presented in Fig. 2a, the intense identified reflections observed at $2\theta = 19.2°$, 37.3°, 39.0°, 45.4°, 60.0°, 66.0°, 66.2°, and 69.6° could be assigned to (111), (311), (222), (400), (331), (333), (440) and (531) reflections of spinel structure $LiCoO_2$ with space group Fd3m (JCPDS card, No.44–0145), respectively.[24] Notably, no splitting in reflections at ~39.0° and 66.2° are found, as is characteristic of the lower temperature synthesis of the LT-LCO phase, distinctly different from HT-LCO phases grown at the normal higher temperatures, where the former separates to (006) and (012) reflections and the latter comprise (018) and (110) reflections.[14,51–53] Moreover, the position of the main (111) reflection shifts to a higher angle ($2\theta = 19.2°$; HT-LTO at 18.5°), which is specific to LT-LCO.[19] In addition, the relatively low intensity peaks at 2θ = 32.3°, 36.8° and 55.7° are from (220), (311) and (422) planes of Co_3O_4 (JCPDS card, No.78–1970).[54,55] The cubic spinel structure of Co_3O_4 from thermal decomposition of the $[Li_2(ox)_2][Co_5(OH)_8]$ LDH occurs with the crystallization of stoichiometric $LiCoO_2$. We note that there is no contributory phase of HT-LCO evidenced by splitting in reflections, or Li_2CO_3 as is often found using other synthetic methods for LT-LCO.

The modified LT-LCO materials exhibit strong similarity in their XRD patterns to the as-synthesized LT-LCO materials, including the $LiCoO_2$ phase and secondary Co_3O_4 phase. The surface coating and doping phases formed here are amorphous, and it has been established that AlF_3 forms in an amorphous state. The coating does not modify the crystallinity of the underlying LT-LCO phase. In comparison, there are stronger intensities of (311) and (400) reflections and a weaker (111) reflection in the modified LT-LCO material consistent with coating of the particle outer surface with an amorphous layer and introduction of the AlF_3 phase into the material. The surface modification with $LiAlO_2$ and AlF_3 can cause migration of the fluoride phase into the LT-LCO resulting in an expansion of unit cell axes. Other studies on Mn-rich layered cathode materials have shown that partial diffusion of Al^{3+} ions from AlF_3 can diffuse into the bulk, modifying the intensity the XRD reflections of the LT-LCO phase.[48] Such an effect from Al^{3+} ingress is not found in our case. The thin coating layer volume was not sufficient for detection by PXRD, but its composition is examined using higher resolution electron microscopy further on.

We also used Raman scattering spectroscopy to distinguish between phases of different crystal symmetries on the basis of various Raman active vibrational modes. Typically, there are two main Raman bands at O–Co−O bending at 490 cm^{-1} (E_g) and Co −O stretching at 597 cm^{-1} (A_{1g}) for rhombohedral LCO with R3m symmetry, which is the phase of LCO originally reported by Goodenough et al. in 1980[5] while there are four various modes for spinel LCO with cubic symmetry (Fd3m) at 480, 525, 621, and 690 cm^{-1}, arising from $2F_g$, E_g, A_{1g} phonons.[56] These modes are typical of LCO formed at lower temperature.[14] As displayed in Fig. 2b, each LCO crystal structure gives rise to a specific Raman

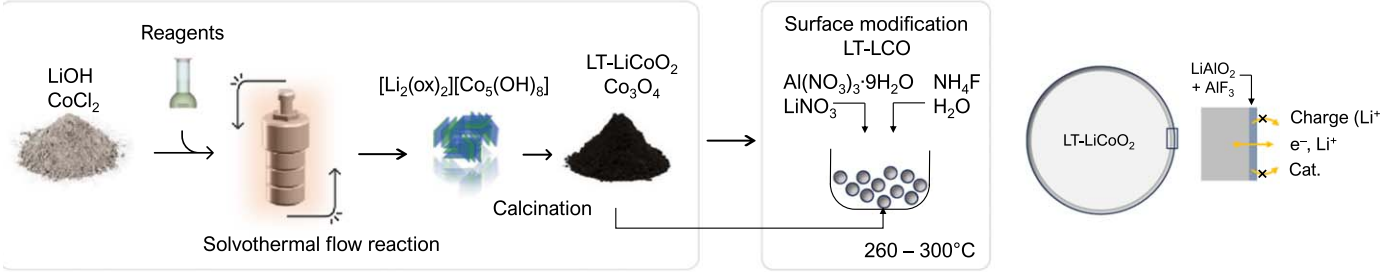

Figure 1. Synthesis of LT-LCO from either pure reactants or recycled battery material ashes achieved using solvothermal flow reactions to form a layered double hydroxide. Calcination at 300 °C gives the LT-LCO products. Surface modification subsequently coats the LT-LCO particles in a layer containing $LiAlO_2$ and AlF_3. The schematic on the right proposes that the layer, while being ionically conductive (e^-, Li^+), limits Li/O migration or catalysis with the electrolyte (Cat.) and mitigates LCO decomposition during charge (Charge (Li^+)).

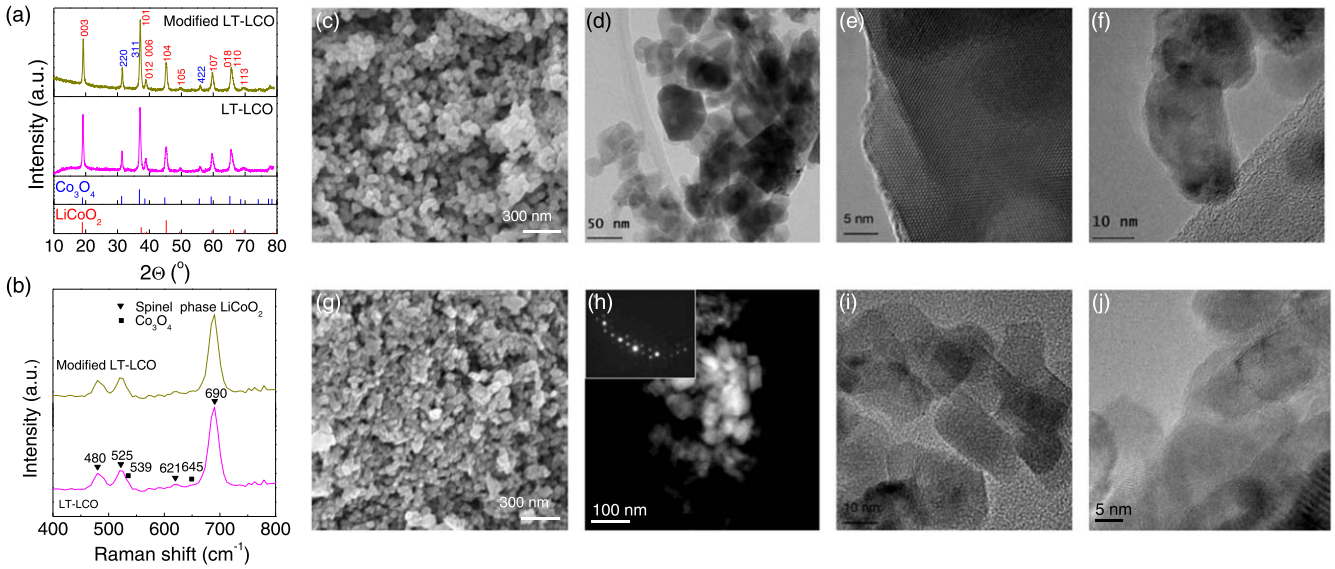

Figure 2. (a) XRD pattern for the calcined LT-LCO powder and the modified LT-LCO material. Reference patterns for Co_3O_4 and $LiCoO_2$ in cubic phase are also shown. (b) Raman scattering spectra for LT-LCO samples and modified LT-LCO powder. (c) SEM images and (d-f) bright field TEM and HRTEM images of the as synthesized LT-LCO powder. (g) SEM and (h-j) TEM images of the modified LT-LCO samples. The TEM mage in (h) is a high angle annular dark field image of several nanocrystals of the modified LT-LCO and corresponding nanobeam diffraction pattern (inset).

fingerprint, four strong Raman bands at 480, 525, 621, and 690 cm^{-1} correspond to the existence of spinel phase LCO, whereas two small bands at 539 and 645 cm^{-1} may be attributed to the presence of a small amount of the secondary Co_3O_4 phase with low crystallinity.[25] Previous reports have ascribed these modes to cation mixing in this phase, but other investigations have questioned the validity of cation mixing, and instead arise from two distinct spinel phases: the spinel LT-LCO and a spinel $Li_{0.5}CoO_2$. These similarity of the Raman bands in both materials indicates that LT-LCO materials and modified LT-LCO materials are composed primarily of spinel LCO phase and a small amount of a separate Co_3O_4 phase, and the modification of the materials did not adversely affect the crystal structure. An expectation from this work was that the $[Li_2(ox)_2][Co_5(OH)_8]$ LDH structural pre-organisation of alternating lithium and cobalt layers would allow for the rhombohedral form of $LiCoO_2$ to form at low temperature. However the LT-LCO material is predominantly spinel structure. The modification and coating of the LT-LCO was developed to ensure its performance was improved to be somewhat comparable to rhombohedral LCO.

The morphologies of LT-LCO materials from SEM and TEM examination before and after modification are displayed in Figs. 2c–2f. We observe no significant changes in general morphology due to modification. The particles LT-LCO and Co_3O_4 that show faceted structure maintain their overall shape without serious agglomeration. The primary difference is that the modified LT-LCO materials appear slightly rougher owing to the addition of the surface layers (detailed further on) whereas the bare LT-LCO materials have a clean-faceted surface morphology. Post modification (Figs. 2g–2j) shows similar structures with additional surface coating, and the dark field image with corresponding nanobeam diffraction confirm the cubic structure and crystallinity of the product.

Transmission electron microscopy (TEM) and high resolution TEM (HRTEM) was performed to further investigate the morphologies and chemical composition of the LT-LCO material (Fig. 2). The electron micrographs of the LT-LCO material consisted predominantly of faceted grains with clear well-defined facets and some irregular nanoparticles. These grains display a size of ∼30–-50 nm and nanoparticles are ∼10–30 nm (Figs. 2d–2f). Some nanoscale particles with random relative orientation were too small in our system to obtain a single phase crystal electron diffraction patterns. After surface coating modification, the particles appear similar in size and shape, where the spinel LT-LCO cubic grains are dominant and mixed with some Co_3O_4 nanoparticles[57] (Fig. 2g). The crystallinity is maintained after modification evidenced by the nanobeam diffraction measurements from high angle annular dark field imaging of the spinel LT-LCO phase.

High resolution scanning transmission electron microscopy examination of the constituent crystalline materials show finer detail of their structure, particularly post modification. In Fig. 3a, we see the well-faceted cubic-shaped grains that are Co_3O_4 from HAADF-STEM images. Along this zone axis we can see clear Co atomic columns characteristic of this phase. The dark field images and FFT patterns in Figs. 3b, 3c shows an antiphase boundary from the edge of single crystal of the LT-LCO material. The LT-LCO crystals are also of high crystalline quality. The individual grains show continuous lattice fringes with d-spacings of 0.25 nm and 0.45 nm, which correspond to (311) and (111) planes of spinel LCO, respectively.[58] Close observation shows an ultrathin amorphous coating layer of ∼5–10 nm on the surface after modification (Figs. 3d–3f).

The underlying LT-LCO crystal size and phase remain more or less similar to the as-synthesized material, and so we used X-ray photoelectron spectroscopy (XPS) explicitly check the chemical content of the as-synthesized and modified LT-LCO (Figs. 4 and S1). The core-level photoemission measurements verified the introduction of F and Al in the modified LT-LCO materials by comparison of LT-LCO before and after modification (Fig. S1a). The Co 2p core-level spectra in Fig. 4a provides information on the surface composition including the modifier coating and the LCO and Co_3O_4 particles. The Co $2p_{3/2}$ at 781.4 eV and its satellite at 789.7 eV (Fig. 4a), Co $2p_{1/2}$ at 789.2 eV and its satellite at 805.2 eV (Fig. 4a), and Co 3p at 60.9 eV (Fig. S1b), together with the presence of a lithium peak at 54.1 eV (Fig. S1b) are strong evidence for the existence of the LCO phase.[56,59] We observe a shift in the 2p core levels to lower binding energy after modification consistent with the surface coating reducing the overall oxidation state of the transition metal (in this case Co). The XPS data here is consistent with other reports of the reduction of some Co^{3+} by F^- (from dissociated AlF_3 on the surface) and associated charge compensation that allow Co^{3+} reduction. In tandem, expansion of the transition metal slab in the crystal structure has been postulated due to introduction of F^- that improves intercalation and mitigates voltage fading and capacity loss

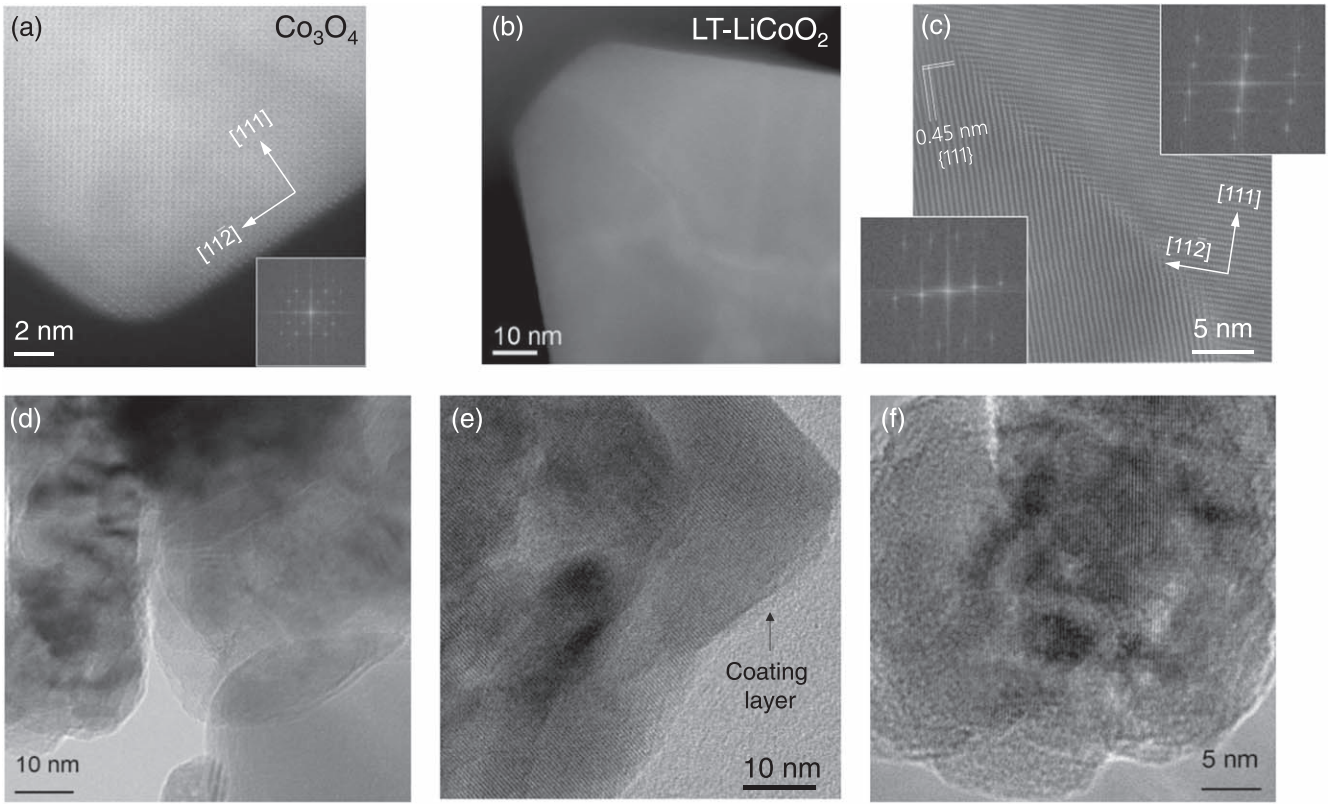

Figure 3. (a) HAADF-STEM image of a Co_3O_4 nanocrystal with corresponding FFT pattern. (b) HAADF-STEM image of the LT-LCO crystalline material, with cubic spinel structure. The image in (c) shows an antiphase boundary for this particular crystal. (d-f) Bright field HRTEM data of crystalline LT-LCO material taken after modification, showing the thin amorphous surface coating of all particles.

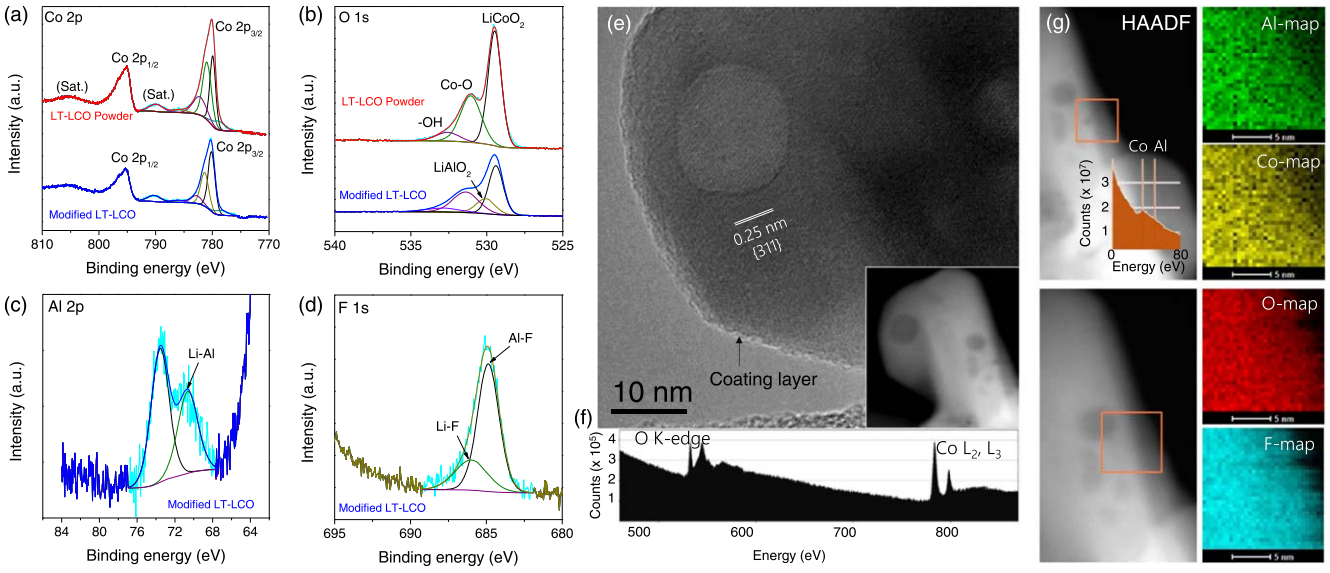

Figure 4. XPS core-level spectra of as-synthesized and modified LT-LCO powder showing (a) Co 2p, (b) O 1s, (c) Al 2p and (d) F 1s. The comparison between core-level emission from as-made and modified LT-LCO are shown in (a) Co 2p and (b) O 1s. (e) Bright field HRTEM image of a single modified LT-LCO particle with a dark field STEM image (inset). (f) EELS spectrum of the O K-edge and Co $L_{2,3}$ edge. (g) A pair of HAADF-STEM images of a region from the modified LT-LCO particle shown in (e) with corresponding EELS maps of Al, Co, O and F. Al and C are mapped from the orange box in the upper STEM image; O and F are mapped from the orange box in the lower STEM image. (Inset) EELS spectrum showing Co and Al presence.

over time. Since the Al is maintained at the surface in the $LiAlO_2$ coating, shrinkage of the transition metal slabs in the spinel phase is less likely, since it would imply Al^{3+} introduction into the LT-LCO, which would worsen the overall electrochemical response. The Co $2p_{3/2}$ peak at 780.1 eV, Co $2p_{1/2}$ peak at 782.8 eV (Fig. 4a) and O1s peak (Fig. 4b) at ~531 eV stem from the Co_3O_4 phase.[59] For the O 1s core-level (Fig. 4b), the strong peak at 529.5 eV is attributed to typical characteristic of O atoms in the spinel phase LT-LCO crystal.

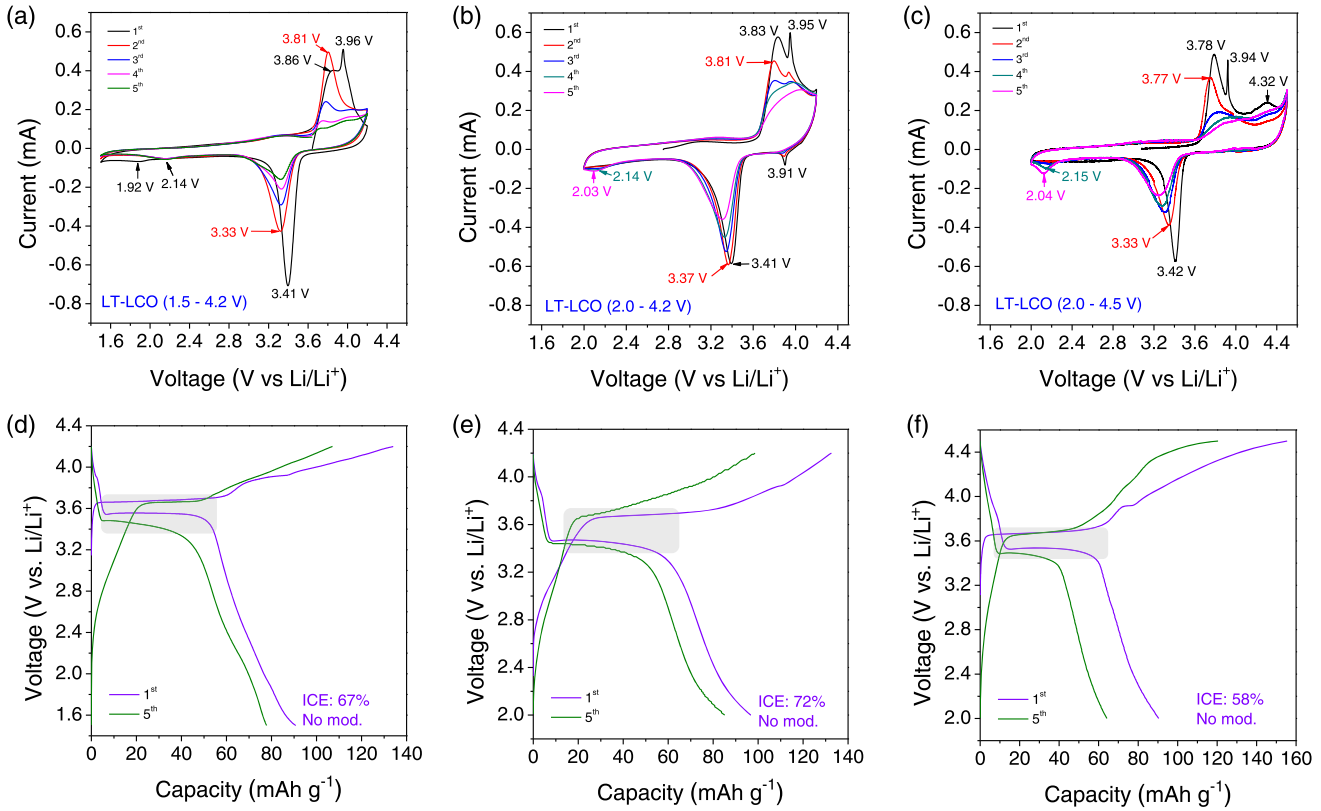

Figure 5. First through fifth cycle in CV curves in the voltage range (a) 1.5–4.2 V, (b) 2.0–4.2 V and (c) 2.0–4.5 V (vs Li/Li^+) at scan rates of 0.05 mV s^{-1} and the galvanostatic charge-discharge curves corresponding to 1st and 5th cycle with the operating voltage range of (d) 1.5–4.2 V, (e) 2.0–4.2 V and (f) 2.0–4.5 V (vs Li/Li^+) at a lower current density of 0.02 C (1 C = 200 mA g^{-1}) rate for the as-synthesized LT-LCO electrode.

The lowest energy peak (532.6 eV) relates to weakly adsorbed O species on the surface including bound surface water/hydroxyls/organic, or CO_3^{2-} surface impurities.[60]

The O 1s (Fig. 4b and Al 2p (Fig. 4c) peaks at binding energies of 530.1 eV and 73.6 eV are assigned to $LiAlO_2$, rather than Al_2O_3 because of the lower electronegativity of Li with respect to Al.[39,40] As a material with high Li-ion conductivity, $LiAlO_2$ as the modification layer promotes lithium ion diffusion kinetics for LT-LCO, and prevents Li and O loss from the material during cycling.[61,62] The F 1s core level photoemission in Fig. 4d at 684.9 eV may be ascribed to the introduction of AlF_3 into the LT-LCO compound, and we see some evidence of Li-F interactions together with Al-F, consistent with $LiAlO_2$ and AlF_3.[40,49] These results confirm that the LT-LCO material comprises an LCO phase and secondary Co_3O_4 phase as separate crystalline contents; the modification layer coats the crystalline particles and contains $LiAlO_2$ and AlF_3.

The bright field TEM image in Fig. 4e and corresponding HAADF-STEM images of the same region were analyzed by electron energy loss spectroscopy. The EELS spectrum in Fig. 4f confirms Co and O in the material consistent with literature spectra for $LiCoO_2$. Obtaining detailed EELS for the Li K-edge was not possible due to overlap with the $M_{2,3}$ spectra of Co in the low-loss energy range, and also the spectra overlap with Al. EELS mapping of the outer surface and edges of the modified LT-LCO material were acquired for Co, Al, O and F in the high-loss energy regions, including Co $L_{2,3}$ exhibiting a Co^{3+} oxidation state. These EELS maps are shown in Fig. 4g together with the corresponding HAADF-SEM images and the regions of interest for mapping. The presence of all four elements is confirmed in the outer coating following modification. For F- and O-detection by EELS, the detector CCD pixels were binned to improve signal-to-noise form the thin outer coating, and all four elements were clearly detected from integrated spectra. Together with the XPS data, it confirms there presence of $LiAlO_2$ and AlF_3 after modification.

Electrochemical behavior of the modified LT-LCO cathode material.—To explore the lithium storage mechanism of the LT-LCO and modified LT-LCO materials, cyclic voltammetry (CV) was carried out at a scan rate of 0.05 mV s^{-1} under different voltage ranges, including 1.5–4.2 V, 2.0–4.2 V and 2.0–4.5 V (vs Li/Li^+). As shown in Figs. 5a–5c for the as-made LT-LCO materials, in the initial anodic and cathodic scan, there are two pairs of oxidation/reduction peaks between 3.3 and 4.0 V, which are characteristic of the spinel LT-LCO structure.[16,17] The broad peak at ~2.0 V is associated with the Co_3O_4 phase. Two defined oxidation peaks at 3.86 V and 3.96 V indicates a two-step lithium extraction process from the spinel LCO octahedral sites, while a distinct reduction peak at 3.41 V and the minor one at 3.91 V may be attributed to the insertion of Li^+ into octahedral sites and tetrahedral sites of the spinel structure, respectively. On continuous voltammetric scans, the reduction peak at 3.41 V shifts to a lower voltage, demonstrating a change in the site energy of the octahedral sites.[17] The disappearance of redox peaks at 3.91 V indicates some irreversibility of lithium storage in the tetrahedral sites. The rapid suppression of the redox peak currents that represent insertion/removal at the octahedral sites, illustrates the instability of spinel structures during cycling. By comparison with voltammetric scans between 2.0–4.2 V, the peak shifts and reduction in peak current values are more pronounced in voltammetric scan with a lower cut-off voltage (1.5 V, Fig. 5a) and also when the upper voltage limit is extended to 4.5 V (Fig. 5c).

This phenomenon also appears in initial galvanostatic charge/discharge curves of the LT-LCO samples (Figs. 5d–5f). Similar plateaus are observed in different voltage ranges. The sloped discharge plateau between 2.0–2.5 V is ascribed to the Li reaction with secondary Co_3O_4. The long stable charge/discharge plateau

(near 3.8 V and 3.4 V vs Li^+/Li) and the short charge plateaus (~4.0 V and 3.9 V vs Li^+/Li) generally result from a two-step process of lithium ion extraction/insertion that characteristic for spinel structured LCO cathodes, and in agreement with the CV data. The short potential plateaus disappear and the specific capacity loss that occurs in the fifth cycle results from the instability of the spinel structure from a known irreversible phase transition in the LT-LCO materials. Meanwhile, the lower coulombic efficiency, a larger capacity loss and severe polarization effects are found when using the low voltage limit (Fig. 5d) or higher upper cut-off voltage (Fig. 5f). Thus, an optimum cycling voltage from LT-LCO electrodes is between 2.0 and 4.2 V.

Under the optimum voltage range of 2.0–4.2 V, the electrochemical behavior of LT-LCO cathode and modified LT-LCO cathode was explored and compared. As shown in Fig. 6a, similar to LT-LCO electrode, the distinct initial anodic (3.78 V and 3.93 V) and corresponding cathodic peaks (3.48 V and 3.91 V) are seen in CV curves for the modified LT-LCO electrode, indicative of lithium ion reactions with spinel LCO structure. Another peak at ~2.20 V remains from the secondary cobalt oxide. It is worth mentioning that two oxidation peaks are still maintained after the first CV scan, which indicates that two-stage oxidation process is somewhat reversible and the stability of spinel LCO structure is improved after modification with $LiAlO_2$ and AlF_3. Under voltammetric conditions, the modified LT-LCO shows a smaller voltage difference ΔE between oxidation and reduction processes and the peak current values are not suppressed to the same extent as for unmodified electrodes. The modification to the surface of the LT-LCO by $LiAlO_2$ and AlF_3 clearly improves Li^+ intercalation into the LCO lattice as measured by the reaction rate (current) in the voltammetric response.

The representative galvanostatic discharge-charge voltage profiles for modified LT-LCO electrodes are provided in Fig. 6b. The discharge/charge plateaus between 3.8 and 4.0 V (vs Li^+/Li) are typical characteristic profiles of Li^+ extraction/insertion from/into spinel LCO electrodes and the sloped discharge plateau below 2.5 V is again from Co_3O_4 phase. These similar plateau characteristics are found the galvanostatic discharge-charge curves at a current rates of 0.05 C and 0.5 C (Fig. S2). Compared with as-synthesized LT-LCO electrodes (Figs. 5d–5f and Fig. S3a), a longer potential plateau between 3.4–4.0 V and a smaller potential difference between discharge and charge potential plateaus are found in modified LT-LCO electrodes, which suggests a higher reversible specific capacity and a lower electrode polarization in LT-LCO electrodes after modification by $LiAlO_2$ and AlF_3. After 50 cycles (Fig. S3a), the main voltage plateaus between 3.4–4.0 V that gradually disappear in as-synthesized LT-LCO electrodes, are maintained in modified LT-LCO electrodes. We also note a remarkable improvement of initial coulombic efficiency (0.02 C: 96% in Fig. 6b; 0.5 C: 95% in Fig. S2a; 0.05 C: 97% in Fig. S2c) is characteristic of this modified LT-LCO material, which is much higher than those of as-made LT-LCO electrodes (0.02 C: 72% in Fig. 6e; 0.05 C: 66% in Fig. S3b). These results verify the surface modification and particle coating helps to mitigate against the deleterious changes to the particles from cycling and promotes more reversible lithium intercalation into the spinel LT-LCO structure coated with $LiAlO_2$ and doping from F^- from the AlF_3. Anodic process from electrocatalytic processes are not observed and the voltage and capacity fade is markedly reduced. The stability in voltammetric and galvanostatic data confirms that the LT-LCO is stable with the surface coatings, and importantly the highly delithiated state is passivated against highly oxygen active charge cathode surface with the electrolyte. Essentially, O_2 gas release from $Li_{1-x}CoO_2$ with corresponding Co oxidation state change that drives cathode decomposition is seemingly mitigated. A high charge capacity (80.2 mAh g^{-1}) and discharge capacity (78.2 mAh g^{-1}) are found in modified

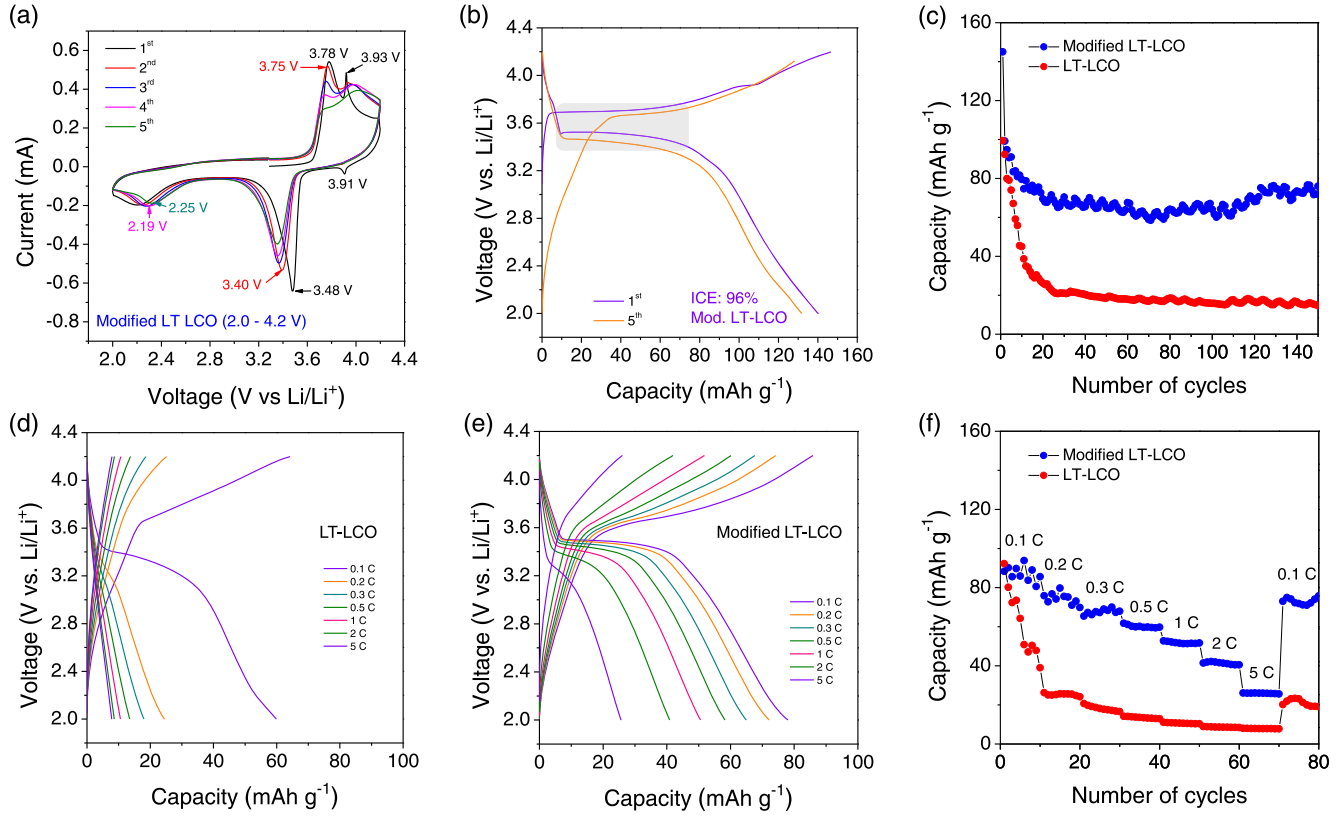

Figure 6. (a) First through fifth cyclic voltammetric cycles at scan rates of 0.05 mV s^{-1}. (b) Galvanostatic charge-discharge curves corresponding to 1st and 5th cycle at a current density of 0.02 C for modified LT-LCO electrodes under the voltage range of 2.0–4.2 V (vs Li^+/Li). (c) Comparison of specific capacity over 150 cycles at a current density corresponding to 0.05 C. (d) Comparison of rate capability at different rates from 0.1 C to 5 C for LT-LCO electrodes and modified LT-LCO electrodes in the voltage range of 2.0–4.2 V.

LT-LCO electrode after 150 cycles, much higher than those (about 20 mAh g^{-1}) of as-synthesized LT-LCO electrodes (Fig. 6c). SEM analysis shows that modified LT-LCO electrode particles are maintained after cycling (Fig. S4) and the surface modification is very beneficial for this phase of low temperature spinel-structured $LiCoO_2$ in maintaining high capacity and stable cyclability. These materials were exposed to ambient condition briefly after cell disassembly prior to analysis, and aside from some agglomeration of the particles, we do not observe any obvious large scale cracking from extended cycling. With $LiAlO_2$ and AlF_3 on the outer surface of the LT-LCO particles, the electrochemical data conclusively shows how the modified material show marked improvements in stability and rate response. Reducing direct contact with the electrolyte is assume here to contribute to this improvement by preventing side reactions from O redox and material degradation.

Rate performance of the modified LT-LCO is also enhanced, as shown in the comparison between Figs. 6d and 6e, where the specific capacities in the range of 80–25 mAh g^{-1} are found at various current densities from 0.1 to 5 C and are markedly improved compared the LT-LCO without any surface modification. Furthermore, a reversible capacity of ∼80 mAh g^{-1} is recovered when the current density returns to 0.1 C (Fig. 6f). In comparison, the specific capacity is reduced to ∼10 mAh g^{-1} a the specific current is increased from 0.5 to 5 C for LT-LCO electrodes (Figs. 6c, 6f) due to the sluggish Li ion transfer kinetics of the unmodified spinel LCO phase, and the capacity is not regained at lower specific currents indicating a severe irreversible degradation of the materials after the maximum investigated rate. Modification with $LiAlO_2$ and AlF_3 mitigates against this degradation and maintains capacity and rate capability. As rate response is fundamentally linked to cation conductivity into the LCO particles without a penalty of increase electronic resistance, we see the surface coating provides this enhancement and ensure stable voltage plateaus consistent with each rate. It is plausible that better access to spinel structure from the F^- from AlF_3 with a stabilized surface with higher ionic mobility $LiAlO_2$, enables this stability and faster kinetics. Additionally, the initial cycles does not suffer from low CE and capacity is fully recovered when the rate is reduced back to 0.1 C.

Remarkably, this material demonstrates a significant improvement in electrochemical lithium storage behavior after $LiAlO_2$ surface layer coating and AlF_3 incorporation compared to bare LT-LCO electrodes directly from a low temperature calcination of the product of solvothermally synthesized layered double hydroxide $[Li_2(ox)_2][Co_5(OH)_8]$. While the layered form of LCO that is used commercially is the highest performance option, a $LiAlO_2$ lithium ion conductive layer with excess Li and AlF_3 is useful to solve the Li ion diffusion issue of the spinel LT-LCO phase, providing more extensive diffusion pathways for the Li ion extraction/insertion processes with the spinel LT-LCO crystal while stabilizing the interface against activity with the electrolyte. It also provides outstanding initial coulombic efficiency for this type of material. The process is straightforward and allow a low-temperature route to LCO with reasonably good capacity and rate capability that may be useful when considering sources of LCO from recycling from sources other than spent Li-ion batteries. Future work is focused on reducing the amount of companion Co_3O_4 that was maintained in all electrochemical analysis here including specific capacity calculations.

Conclusions

A low temperature route to a stable, coated spinel-phase LT-LCO material with secondary Co_3O_4 phase was synthesised at 300 °C directly from the layered double hydroxide $[Li_2(ox)_2][Co_5(OH)_8]$ product of solvothermally synthesized LiOH and $CoCl_2$. The electrochemical characterization in lithium battery cells demonstrates the reversible lithiation of the LT-LCO spinel phase occurs as a two-step process at lower voltages between 3.3 and 4.0 V. While as-prepared LT-LCO materials have poor cycle and rate performance due to sluggish lithium ion kinetics and the instability of the spinel structure, their modification using surface coatings was developed to mitigate limitations characteristic of spinel-phase LCO. Modification of the cubic LCO particles with an $LiAlO_2$ surface coating and AlF_3 inclusion enhances the reversible lithium storage performance of the LT-LCO material. As a result, modified LT-LCO materials exhibit better cycle life (80 mAh g^{-1} after 150 cycles) and rate behavior, with a considerable improvement in initial coulombic efficiency as high as 95%. These improvements results from the modification of the LCO crystallites with lithium ion-conducting $LiAlO_2$ and AlF_3. This overall method of solvothermal synthesis of precursors to provide LCO materials be extended to materials from recycled Li-ion battery cathodes, and be extended to other cathode materials.

Acknowledgments

We acknowledge support from the European Union's Horizon 2020 research and innovation program under grant agreement No 825114. We also acknowledge support from the Irish Research Council under an Advanced Laureate Award (IRCLA/19/118) and a Government of Ireland Postdoctoral Fellowship (GOIPD/2021/438). V. N. and A. R. wish to acknowledge the support of the ERC CoG, 3D2DPrint (681544), SFI AMBER (12/RC/2278_P2) and SFI FFT R21/196. They would also like to acknowledge the SFI-funded CRANN Advanced Microscopy Laboratory (AML) for the provision of their facilities for the microscopy characterization and analysis. This work has also emanated from research conducted with the financial support of Science Foundation Ireland under Grant number 19/FIP/ZE/7567 R and is co-funded by the Department for Foreign Affairs.

ORCID

Colm O'Dwyer https://orcid.org/0000-0001-7429-015X

References

1. J.-M. Tarascon and M. Armand, *Nature*, **414**, 359 (2001).
2. B. Dunn, H. Kamath, and J.-M. Tarascon, *Science*, **334**, 928 (2011).
3. J. B. Goodenough and Y. Kim, *Chem. Mater.*, **22**, 587 (2010).
4. D. Larcher and J. M. Tarascon, *Nat. Chem.*, **7**, 19 (2015).
5. K. Mizushima, P. C. Jones, P. J. Wiseman, and J. B. Goodenough, *Mater. Res. Bull.*, **15**, 783 (1980).
6. M. Armand and J. M. Tarascon, *Nature*, **451**, 652 (2008).
7. K. Wang, J. Wan, Y. Xiang, J. Zhu, Q. Leng, M. Wang, L. Xu, and Y. Yang, *J. Power Sources*, **460**, 228062 (2020).
8. W. D. Johnston, R. R. Heikes, and D. Sestrich, *J. Phys. Chem. Solids*, **7**, 1 (1958).
9. T. Tsuruhama, T. Hitosugi, H. Oki, Y. Hirose, and T. Hasegawa, *Appl. Phys. Express*, **2**, 085502 (2009).
10. E. Plichta, M. Salomon, S. Slane, M. Uchiyama, D. Chua, W. B. Ebner, and H. W. Lin, *J. Power Sources*, **21**, 25 (1987).
11. J. N. Reimers and J. R. Dahn, *J. Electrochem. Soc.*, **139**, 2091 (1992).
12. M. D. Bhatt and C. O'Dwyer, *Phys. Chem. Chem. Phys.*, **17**, 4799 (2015).
13. M. D. Bhatt and C. O'Dwyer, *Curr. Appl Phys.*, **14**, 349 (2014).
14. R. J. Gummow, M. M. Thackeray, W. I. F. David, and S. Hull, *Mater. Res. Bull.*, **27**, 327 (1992).
15. R. J. Gummow, D. C. Liles, M. M. Thackeray, and W. I. F. David, *Mater. Res. Bull.*, **28**, 1177 (1993).
16. E. Rossen, J. N. Reimers, and J. R. Dahn, *Solid State Ionics*, **62**, 53 (1993).
17. R. J. Gummow, D. C. Liles, and M. M. Thackeray, *Mater. Res. Bull.*, **28**, 235 (1993).
18. C. Wolverton and A. Zunger, *J. Electrochem. Soc.*, **145**, 2424 (1998).
19. O. A. Brylev, O. A. Shlyakhtin, T. L. Kulova, A. M. Skundin, and Y. D. Tretyakov, *Solid State Ionics*, **156**, 291 (2003).
20. T. Maiyalagan, K. A. Jarvis, S. Therese, P. J. Ferreira, and A. Manthiram, *Nat. Commun.*, **5**, 3949 (2014).
21. B. Garcia, J. Farcy, J. P. Pereira-Ramos, and N. Baffier, *J. Electrochem. Soc.*, **144**, 1179 (1997).
22. Y. S. Yoon, S. H. Lee, S. B. Cho, and S. C. Nam, *J. Electrochem. Soc.*, **158**, A1313 (2011).
23. M. J. Armstrong, C. O'Dwyer, W. J. Macklin, and J. D. Holmes, *Nano Res.*, **7**, 1 (2014).
24. S. G. Kang, S. Y. Kang, K. S. Ryu, and S. H. Chang, *Solid State Ionics*, **120**, 155 (1999).
25. S. Tintignac, R. Baddour-Hadjean, J.-P. Pereira-Ramos, and R. Salot, *Electrochim. Acta*, **60**, 121 (2012).
26. H. Y. Park, S. C. Nam, Y. C. Lim, K. G. Choi, K. C. Lee, G. B. Park, H. P. Kim, and S. B. Cho, *Korean J. Chem. Eng.*, **23**, 832 (2006).
27. J.-P. Brog et al., *Journal of Nanobiotechnology*, **15**, 58 (2017).
28. Z. S. Peng, C. R. Wan, and C. Y. Jiang, *J. Power Sources*, **72**, 215 (1998).

29. I.-H. Oh, S.-A. Hong, and Y.-K. Sun, *J. Mater. Sci.*, **32**, 3177 (1997).
30. B. Garcia, J. Farcy, J. P. Pereira-Ramos, J. Perichon, and N. Baffier, *J. Power Sources*, **54**, 373 (1995).
31. A. Burukhin, O. Brylev, P. Hany, and B. R. Churagulov, *Solid State Ionics*, **151**, 259 (2002).
32. S. Mao, Z. Shen, W. Zhang, Q. Wu, Z. Wang, and Y. Lu, *Adv. Sci.*, **9**, 2104841 (2022).
33. X. Yang et al., *Adv. Energy Mater.*, **12**, 2200197 (2022).
34. M. Yoon et al., *Adv. Funct. Mater.*, **30**, 1907903 (2020).
35. S. Kalluri, M. Yoon, M. Jo, S. Park, S. Myeong, J. Kim, S. X. Dou, Z. Guo, and J. Cho, *Adv. Energy Mater.*, **7**, 1601507 (2017).
36. P. Guan, L. Zhou, Z. Yu, Y. Sun, Y. Liu, F. Wu, Y. Jiang, and D. Chu, *Journal of Energy Chemistry*, **43**, 220 (2020).
37. J. Zhang, R. Gao, L. Sun, H. Zhang, Z. Hu, and X. Liu, *Electrochim. Acta*, **209**, 102 (2016).
38. Y. Wang et al., *Adv. Energy Mater.*, **10**, 2001413 (2020).
39. J. Qian, L. Liu, J. Yang, S. Li, X. Wang, H. L. Zhuang, and Y. Lu, *Nat. Commun.*, **9**, 4918 (2018).
40. J. Xie et al., *ACS Nano*, **11**, 7019 (2017).
41. N. Phattharasupakun, C. Geng, M. B. Johnson, R. Väli, A. Liu, Y. Liu, M. Sawangphruk, and J. R. Dahn, *J. Electrochem. Soc.*, **167**, 120531 (2020).
42. G. Kaur and B. D. Gates, *J. Electrochem. Soc.*, **169**, 043504 (2022).
43. M. Cai et al., *Nat. Energy*, **8**, 159 (2023).
44. Y. Fan et al., *Angew. Chem. Int. Ed.*, **62**, e202213806 (2023).
45. W. Jiang, C. Zhang, Y. Feng, B. Wei, L. Chen, R. Zhang, D. G. Ivey, P. Wang, and W. Wei, *Energy Storage Mater.*, **32**, 37 (2020).
46. K. Hu, G. Lv, J. Zhang, X. Guo, Z. Wu, W. Xiang, X. Lan, K. Zhou, P. Xu, and L. Zhang, *ACS Appl. Mater. Interfaces*, **12**, 42660 (2020).
47. Z. Zhu, R. Gao, I. Waluyo, Y. Dong, A. Hunt, J. Lee, and J. Li, *Adv. Energy Mater.*, **10**, 2001120 (2020).
48. P. Vanaphuti, Y. Liu, X. Ma, J. Fu, Y. Lin, J. Wen, Z. Yang, and Y. Wang, *ACS Appl. Mater. Interfaces*, **13**, 22597 (2021).
49. W. Kong, J. Zhang, D. Wong, W. Yang, J. Yang, C. Schulz, and X. Liu, *Angew. Chem. Int. Ed. Engl.*, **60**, 27102 (2021).
50. *A lithium metal oxide and a precursor for the synthesis thereof*, GB2118027.8 (2021).
51. J.-Y. Park, C. H. Hwang, M.-H. Choi, J.-E. Kim, K. M. Ok, and I.-W. Shim, *Bull. Korean Chem. Soc.*, **31**, 327 (2010).
52. M. Antaya, J. R. Dahn, J. S. Preston, E. Rossen, and J. N. Reimers, *J. Electrochem. Soc.*, **140**, 575 (1993).
53. C.-L. Liao and K.-Z. Fung, *J. Power Sources*, **128**, 263 (2004).
54. C.-W. Wang et al., *Energy Environ. Sci.*, **14**, 437 (2021).
55. S. Mao, Z. Shen, W. Zhang, Q. Wu, Z. Wang, and Y. Lu, *Adv. Sci.*, **9**, 2104841 (2022).
56. S.-W. Song, K.-S. Han, and M. Yoshimura, *J. Am. Ceram. Soc.*, **83**, 2839 (2000).
57. W. M. Seong, K. Yoon, M. H. Lee, S.-K. Jung, and K. Kang, *Nano Lett.*, **19**, 29 (2019).
58. B. Garcia, P. Barboux, F. Ribot, A. Kahn-Harari, L. Mazerolles, and N. Baffier, *Solid State Ionics*, **80**, 111 (1995).
59. K. L. Browning, L. Baggetto, R. R. Unocic, N. J. Dudney, and G. M. Veith, *J. Power Sources*, **239**, 341 (2013).
60. L. Dahéron, H. Martinez, R. Dedryvère, I. Baraille, M. Ménétrier, C. Denage, C. Delmas, and D. Gonbeau, *J. Phys. Chem. C*, **113**, 5843 (2009).
61. Y. Hu, A. Ruud, V. Miikkulainen, T. Norby, O. Nilsen, and H. Fjellvåg, *RSC Adv.*, **6**, 60479 (2016).
62. J. S. Park, X. Meng, J. W. Elam, S. Hao, C. Wolverton, C. Kim, and J. Cabana, *Chem. Mater.*, **26**, 3128 (2014).